Journal of Materials Chemistry A

Accepted Manuscript

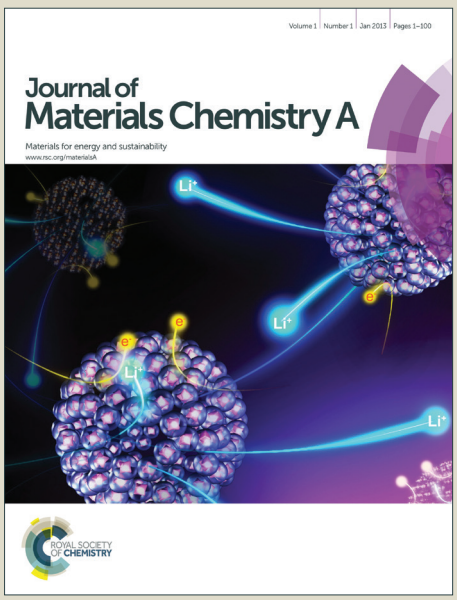

ROYAL SOCIETY OF CHEMISTRY

www.rsc.org/materialsA

Journal of Materials Chemistry A

Cite this: DOI: 10.1039/c0xx00000x

www.rsc.org/xxxxxx

ARTICLE TYPE

Structural Stability of BTTB-based Metal-Organic Frameworks under Humid Conditions

Jagadeswara R. Karra‡, Himanshu Jasuja‡, You-Gui Huang‡, and Krista S.Walton*

Received (in XXX, XXX) Xth XXXXXXXXX 20XX, Accepted Xth XXXXXXXXX 20XX
DOI: 10.1039/c0xx00000x

Stability of metal-organic frameworks (MOFs) under humid environments is of particular interest for their potential commercial and industrial uses. In this work, water vapor adsorption experiments and subsequent structural analysis on the newly synthesized BTTB-based MOFs (BTTB = 4,4',4'',4'''-benzene-1,2,4,5-tetrayltetrabenzoic acid) have been performed to investigate their stability under humid conditions. ZnBTTB and CdBTTB degrade completely after exposure to 90% relative humidity (RH). The instability of ZnBTTB is due to the four-coordinated zinc carboxylate system similar to MOF-5. Similarly, CdBTTB is also unstable as Cd^{2+} ions have coordination number of 4 when the MOF is activated (desolvated). Unlike ZnBTTB and CdBTTB, the structure of ZnBTTBBDC has not degraded significantly upon exposure to 90% RH. This partial structure retention is attributed to the higher nuclearity of metal in the SBU of ZnBTTBBDC and higher metal coordination number compared to ZnBTTB and CdBTTB. Water adsorption isotherms of CoBTTBAZPY and ZnBTTBAZPY show type V behavior due to free nitrogen sites. The crystal structures of AZPY-based pillared MOFs show partial loss of crystallinity whereas BPY-based pillared MOFs remain stable after exposure to 90% RH. The greater stability of BPY-based MOFs is attributed to the higher extent of catenation, higher rigidity of the BPY linker, and absence of any hydrophilic sites.

1. Introduction

Traditional porous materials such as activated carbons and zeolites have been widely used in industry as adsorbents and catalysts for decades.[1] Metal-organic frameworks (MOFs), which consist of metal clusters connected to each other with the help of organic ligands,[2] have emerged as new contenders in the last decade or so.[3] There is significant interest in these materials for adsorption applications because they are chemically tuneable and possess extremely high porosities.[4-9] Hence, MOFs have great potential for use in applications such as catalysis, adsorption-based separations, gas storage, and chemical sensing.[10-18] Many separation applications are complicated by the presence of small quantities of water, which would limit the use of materials with known water sensitivity.

Greathouse and Allendorf reported that MOF-5 dissociates upon contact with water due to ligand displacement at metal sites.[19] Li and Yang found that MOF-177 adsorbs ~ 10 wt% H_2O and is unstable upon exposure to ambient air in 3 days.[20] Liang et al. reported water vapor adsorption studies on (DMOF) $MBDC(DABCO)_{0.5}$ where M= Zn, Ni and found that the structures of the two MOFs are stable up to 30% relative humidity (RH), but collapsed after 60% RH.[21] Kondo et al. investigated water adsorption on three-dimensional (3-D) pillared-layer MOFs $Cu_2(pzdc)_2(pyz)$, $Cu_2(pzdc)_2(bpy)$, and $Cu_2(pzdc)_2(bpe)$. These MOFs were shown to be water resistant, and it was observed that as the pillared ligand becomes longer, the water adsorption amount is larger.[22] Kusgens et al. measured water adsorption isotherms for CuBTC, ZIF-8, MIL-100 (Fe), and DUT-4 and found that ZIF-8, MIL-100 (Fe), and MIL-101 were water stable.[23] Schoenecker et al.[24] investigated the water vapor adsorption properties and subsequent structural analysis of several well-known MOFs: Mg-MOF-74, UiO-66, UMCM-1, DMOF, Cu-BTC, DMOF-NH_2, UMCM-1-NH_2, and UiO-66-NH_2. Among these MOFs, only UiO-66 and UiO-66-NH_2 were found to be completely stable. Low et al.[25] investigated the steam stability of several well-known MOFs at various saturations and temperatures and found that strength of the bond between metal oxide cluster and the bridging linker is important in determining the hydrothermal stability of the MOFs.[25] Hence, carboxylate-based MOFs (MOF-5, MOF-177, UMCM-1) are less water stable than nitrogen (N)-coordinated MOFs such as pillared MOFs, imidazolate, and pyrazolate ligand based MOFs due to the lower basicity of carboxylate ligands.[25,26] However, MOFs such as Cr-based MIL materials (MIL-53,101) and Zr-based UiO-66 materials are notable exceptions to this trend. These MOFs are stable due to inertness of Cr(III) metal[27] and high coordination number and high nuclearity of the Zr-based SBU.[28-31]

Several studies have emerged where researchers have tried to isolate the factors that influence the stability/ instability of MOFs by performing systematic water adsorption studies on isostructural MOF families. Liu et al.[32] and Tan et al.[33] examined the effect of the metal incorporated on the stability in MOF-74

School of Chemical & Biomolecular Engineering,
Georgia Institute of Technology, Atlanta, Georgia, 30332, USA.
E-mail: krista.walton@chbe.gatech.edu;
Fax: +1-404-894-2866; Tel: +1-404-894-5254

‡These authors contributed equally to this work.

†Electronic Supplementary Information (ESI) available. See DOI: 10.1039/c0xx00000x

and DMOF systems respectively. Both of these studies show that Ni-DMOF and Ni-MOF-74 are less susceptible to hydrolysis since Ni^{2+} has the lowest standard reduction potential and hence, it is less prone to react with water.[32] Due to similar reasons it has been reported that water stability of MOF-5 increases upon doping with Ni^{2+} during synthesis.[34] Water stability of Zn-based DMOF has been tuned by functionalization of the BDC ligand.[35] It has been shown that the kinetically unstable DMOF structure maintains its structure upon inclusion of the tetramethyl-BDC ligand even when it adsorbs large amounts of water vapor during cyclic water adsorption experiments. These methyl groups prevent water molecules from clustering near the metal-ligand coordination site.[36] Decoste et al.[37] showed that double-ring Zr-MOFs are less stable than single-ring Zr-MOFs due to steric and rotational effects. These systematic studies give more insight into the inherent stability of MOF structures than reported previously where MOF stability in humid environments is enhanced by merely increasing the hydrophobicity.[38-43] Recently, Burtch et al.[44] reviewed the state of the art in the water stability of MOFs and provided a ranking of MOFs as per their water stability. While the appearance of water-stable MOFs in the literature has been accelerating in recent years,[44] understanding the factors that lead to stability or instability is an important undertaking that will facilitate the use of MOFs at the applied level.

To further address the issue of water stability of MOFs, a systematic study of the effect of water vapor on the newly synthesized BTTB (4,4',4'',4'''-benzene-1,2,4,5-tetrayltetrabenzoic acid, Fig. 1) based MOFs, **CdBTTB, NiBTTB, ZnBTTB, ZnBTTBBDC, ZnBTTBBPY, CoBTTBBPY, ZnBTTBAZPY,** and **CoBTTBAZPY** is reported here. Metal atoms in CdBTTB, NiBTTB, and ZnBTTBBDC are coordinatively unsaturated after complete desolvation. These unsaturated metal centres can coordinate with polar water molecules and can lead to greater water adsorption capacities. NiBTTB has a 2D layered structure while CdBTTB and ZnBTTBBDC are 3D frameworks. The coordination environment in ZnBTTB is different from that of CdBTTB and NiBTTB. The zinc atoms in ZnBTTB are surrounded by oxygen atoms from BTTB ligand and have no open zinc sites. CoBTTBBPY and ZnBTTBBPY are isostructural and can be described as two-fold interpenetrating 3D pillared MOFs with open channels of 4.064 in [0 1 0] direction and 6.044Å in [0 $\bar{1}$ 1] direction. Their frameworks are made from 2D $M_2(BTTB)_4$ sheets which are connected to each other with the help of BPY linker. Thus, BPY acts as a pillar between these 2D sheets. CoBTTBAZPY and ZnBTTBAZPY MOFs are also pillared MOFs but now the AZPY linker acts as a pillar, and these MOFs can also be described as two-fold interpenetrating 3D MOFs with open channels of 1 Å and 4.942 Å in [1 0 0] direction, 4.942 Å in [$\bar{1}$ 1 1] direction and 6.617 Å in [1 0 1] direction. AZPY linkers have free nitrogen coordination sites and can interact preferentially with polar water molecules. Hupp et al.[45] synthesized similar interpenetrated frameworks with pillared-layer structure employing BTTB, BPY and AZPY ligands in DMF and at 80 °C. Despite the same topology, the pore structures and properties are quite different, indicating that solvent and reaction temperature greatly affect the framework structures and properties. Detailed structure description and crystallographic information for the ZnBTTB and NiBTTB MOFs was reported in our previous publication[46] and this information for remaining BTTB-based MOFs is reported in the Electronic Supplementary Information (ESI)†.

This diverse set of structures with differing coordination environments should offer insight into the factors that make MOFs water stable. We expect that among the BTTB MOFs studied here, those constructed with N-based pillared ligands (BPY, AZPY) will be more water stable than MOFs synthesized with only carboxylate-based ligand (BTTB). This stability is attributed to higher basicity of the N-based pyridyl linkers, as compared to typical carboxylate linkers, which results in stronger metal-ligand bonds, and therefore, a purported resistance to hydrolysis by water molecules.[26] Water vapor adsorption equilibria are studied using a gravimetric system. Powder X-ray diffraction (PXRD) and surface area analyses are used to determine structure loss upon exposure to 90% RH.

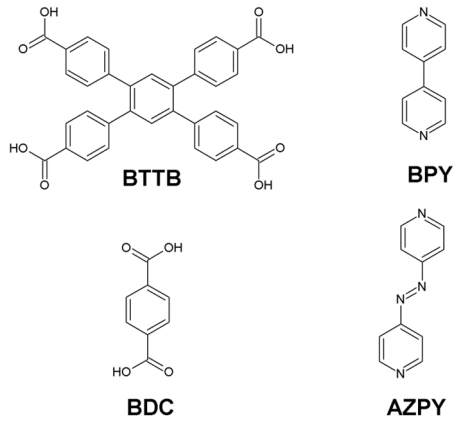

Fig. 1 Organic ligands employed in this work. BTTB = 4,4',4'',4'''-benzene-1,2,4,5-tetrayltetrabenzoic acid; BDC = 1,4-benzenedicarboxylic acid; BPY = bipyridine; and AZPY = azopyridine.

2. Materials Synthesis and Characterization

Synthesis of ZnBTTB and NiBTTB MOFs was performed using a solvothermal method as reported in our previous publication.[46] Detailed synthesis & characterization results for the remaining MOFs (CCDC 986372-986376 contain the supplementary crystallographic data) are reported in the Electronic Supplementary Information (ESI)†. Single-crystal X-ray data were collected on a Bruker APEX II CCD sealed tube diffractometer by using Cu-Kα radiation with a graphite monochromator. The structures were solved by direct methods and refined using the SHELXTL-97 software suite. Powder X-ray diffraction (PXRD) patterns were recorded on a X'Pert X-ray PANalytical diffractometer with an X'accelerator module using Cu Kα (λ = 1.5418 Å) radiation at room temperature, with a step size of 0.02˚ in 2θ. Prior to the adsorption measurements in order to remove guest molecules, the samples were treated under vacuum at their respective activation temperatures (Table 1). Specific surface areas were determined using nitrogen adsorption isotherms on activated MOF samples at -196 °C with a Quadrasorb system from Quantachrome Instruments. BET theory was used to calculate the surface area and was applied over the pressure range suggested for MOFs.[47] Water vapor adsorption

Journal of Materials Chemistry A

Dynamic Article Links ►

Cite this: DOI: 10.1039/c0xx00000x

www.rsc.org/xxxxxx

ARTICLE TYPE

isotherms were measured at 25 °C on samples activated *in situ*, using an Intelligent Gravimetric Analyser (IGA-3 series, Hiden Isochema). Dry air was used as the carrier gas, with a portion of the carrier gas being bubbled through a vessel of deionized water. The relative humidity (RH) was controlled by varying the ratio of saturated air and dry air via two mass flow controllers. Experiments were conducted up to 90% RH due to water condensation in the apparatus at higher humidities. The total gas flow rate was set at 100 cc/min for all the experiments. Each adsorption/desorption step was allowed to approach equilibrium over a period of 2–24 hrs. for each relative humidity point. Nitrogen adsorption isotherms at -196 °C and PXRD patterns were measured again after exposure to water vapor in order to observe the changes in the structures of MOFs. The ligands used in this work are shown in Fig. 1: 4,4',4'',4'''-benzene-1,2,4,5-tetrayltetrabenzoic acid (**BTTB**), 1,4-benzenedicarboxylic acid (**BDC**), bipyridine (**BPY**) and azopyridine (**AZPY**).

3. Results and Discussion

3.1 Characterization

In order to confirm the phase purity of the synthesized MOFs, PXRD experiments were carried out. The experimental and simulated PXRD patterns for each MOF match reasonably well and are shown in the ESI. The properties of the synthesized MOFs along with the BET surface areas before and after water adsorption experiments are reported in Table 1. The values of BET surface areas before and after exposure to 90% RH show that only MOFs NiBTTB, ZnBTTBBPY, and CoBTTBBPY are stable. This point will be revisited in our later discussion.

Figure 2 shows the water vapor adsorption isotherms at 25 °C for CdBTTB, ZnBTTB, and ZnBTTBBDC. The water vapor isotherm for CdBTTB is steeper than that for the ZnBTTB, especially in the lower humidity region. Water vapor is more strongly adsorbed in CdBTTB because of its high affinity with the open cadmium sites. Similarly, ZnBTTBBDC also has slightly higher water loading than ZnBTTB due to open zinc sites. In the higher humidity region, the water loading increases sharply in the case of CdBTTB and ZnBTTB. The desorption branch does not follow the adsorption branch for all three of these MOFs. Hence, large hysteresis is evident in the isotherms, which for MOFs often indicates structural change upon water exposure.[21,22] Hysteresis is smaller in ZnBTTBBDC compared to CdBTTB and ZnBTTB, and we also observe less degradation in ZnBTTBBDC (Table 1, Fig. 3). Furthermore, it can be seen that a significant amount of water is retained in the pores of these MOFs, even when the stream is switched to dry air (0 % RH point in desorption curve). The water vapor capacities at 90% RH are 14.5 mol/kg (26.5 wt %) for CdBTTB, 12 mol/kg (21.6 wt %) for ZnBTTB and 5.2 mol/kg (9.3 wt %) for ZnBTTBBDC. Adsorption capacities near saturation are not dictated by the pore volume here as these MOFs degrade under the adsorption conditions.

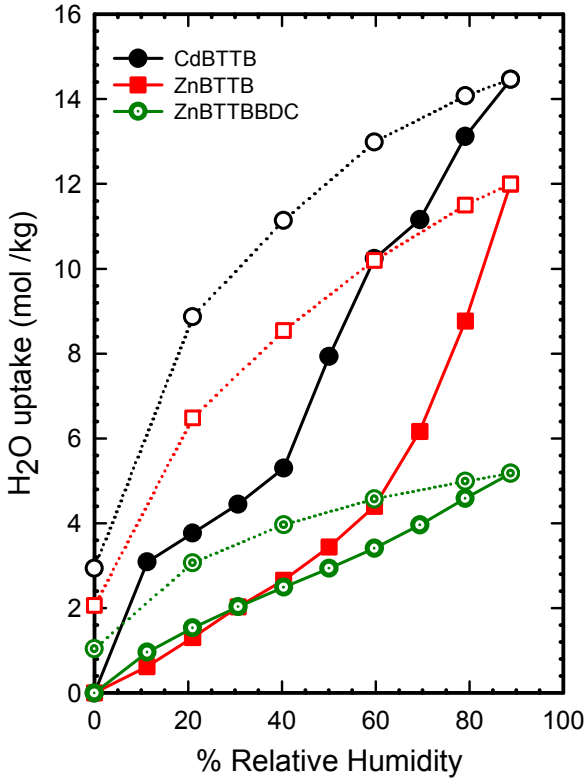

Fig. 2 Water vapor adsorption/desorption isotherms measured at 25°C for desolvated compounds of CdBTTB, ZnBTTB, and ZnBTTBBDC (closed symbols: adsorption; open symbols: desorption). Lines connecting the adsorption points are to guide the eye.

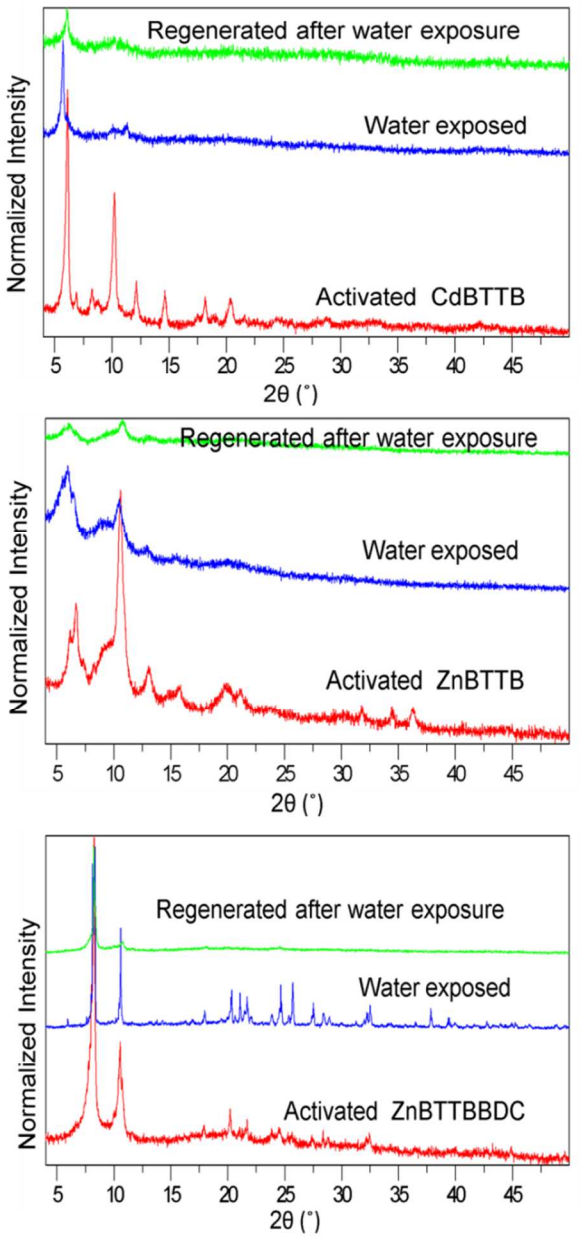

Fig. 3 Powder X-ray diffraction patterns of activated, water exposed, and regenerated CdBTTB, ZnBTTB, and ZnBTTBBDC.

The PXRD patterns of water-exposed CdBTTB, ZnBTTB, and ZnBTTBBDC samples are compared with that of the activated samples in Fig. 3. The PXRD patterns of ZnBTTB and CdBTTB confirm the decomposition of MOF structures upon water exposure. Most of the peaks have disappeared, and the amorphous background has increased. After thermal treatment (regeneration) of water-exposed samples of CdBTTB and ZnBTTB, the PXRD patterns closely match with those of water-exposed samples. Thus, it implies that the decomposition of CdBTTB and ZnBTTB is taking place during water adsorption itself and not during regeneration. Collapse of CdBTTB and ZnBTTB is also confirmed from the surface area (100 % loss) measurements (Table 1). It has been reported in the literature that MOF-5 is unstable due to its 4-coordinated Zn^{2+} ions[25] and therefore, the zinc-oxygen bonds of the BDC linkers are highly susceptible to displacement by the incoming water molecules.[19] Hence, the degradation of ZnBTTB is not surprising, considering it possesses the four-coordinated zinc carboxylate system identical to MOF-5.[19] Similarly, it is not surprising to see that CdBTTB is also not stable as Cd^{2+} ions possess a coordination number of 4 in the activated (desolvated) form of CdBTTB.

Unlike CdBTTB and ZnBTTB, the structure of ZnBTTBBDC has not degraded significantly. ZnBTTBBDC has three different dimetal-carboxylate clusters (high nuclearity of 6 Zn(II) ions in the SBU). The coordination modes of 6 Zn(II) ions in the SBU show diversity, i.e., Zn1, Zn3, and Zn6 are coordinated by four oxygen atoms in a tetrahedral geometry, while Zn2, Zn4, and Zn5 are in a distorted octahedral geometry bonded by six oxygen atoms (Fig. S5, †ESI). Low et al.[25] showed that MOFs with 6-coordinated metal ions tend to be more water stable than those with 4-coordinated metal ions. Moreover, UiO-66 materials have also been shown to be water stable due to high coordination number (8-coordinated) and high nuclearity of the Zr-based SBU (6 Zr(IV) ions in the SBU).[28-31] The PXRD pattern of ZnBTTBBDC after water adsorption experiments and regeneration still shows some of the initial XRD peaks, but other peaks have disappeared, indicating loss of crystallinity and partial collapse of the structure (Fig. 3). BET analysis of the regenerated sample gives surface area loss (Table 1) of 50%, which is consistent with the partial collapse of the structure as indicated by PXRD.

Water vapor adsorption isotherms at 25 ˚C for NiBTTB, ZnBTTBBPY and CoBTTBBPY are shown in Fig. 4. NiBTTB shows slightly higher water vapor loading compared to ZnBTTBBPY and CoBTTBBPY in the low humidity region due to the electrostatic interactions between open nickel sites and water vapor. However, the water loading is very small in this MOF compared to the other open metal site MOFs, CdBTTB and ZnBTTBBDC. One explanation for this observation could be that the 2D net structure and 1D pore channels restrict the diffusion of water molecules. Moreover, the non-polar interactions (hydrophobicity) between BTTB linkers are dominant in the case of NiBTTB that ensured minimal wetting of the pores.

The water adsorption and desorption isotherms in Fig. 4 show complete reversibility (no hysteresis) for NiBTTB and very small hysteresis for CoBTTBBPY and ZnBTTBBPY compared to the water unstable MOFs such as CdBTTB, ZnBTTB, and ZnBTTBBDC. Kondo et al.[22] reported that non-evident hysteresis points to the stability of the framework against water. Moreover, water is not retained in these MOFs when the stream is switched to dry air. This suggests that adsorbed molecules are not strongly bound in these MOFs, as opposed to our observation for water unstable MOFs CdBTTB, ZnBTTB, and ZnBTTBBDC. The adsorption loadings are very small in NiBTTB and CoBTTBBPY MOFs, and the isotherms can be classified as type VII according to IUPAC[48] classification, indicating that these materials are very hydrophobic. CoBTTBBPY and ZnBTTBBPY show similar adsorption loadings till 70% RH due to their isostructural nature and similar pore sizes. However, very high adsorption loadings (9.59 mol/kg at 80% RH, 14.1 mol/kg at 90% RH) are observed for ZnBTTBBPY (Fig. 4) at higher humidities, a significant deviation from the trend shown by CoBTTBBPY. Repeated measurements performed in our lab on ZnBTTBBPY reconfirm

Cite this: DOI: 10.1039/c0xx00000x

www.rsc.org/xxxxxx

ARTICLE TYPE

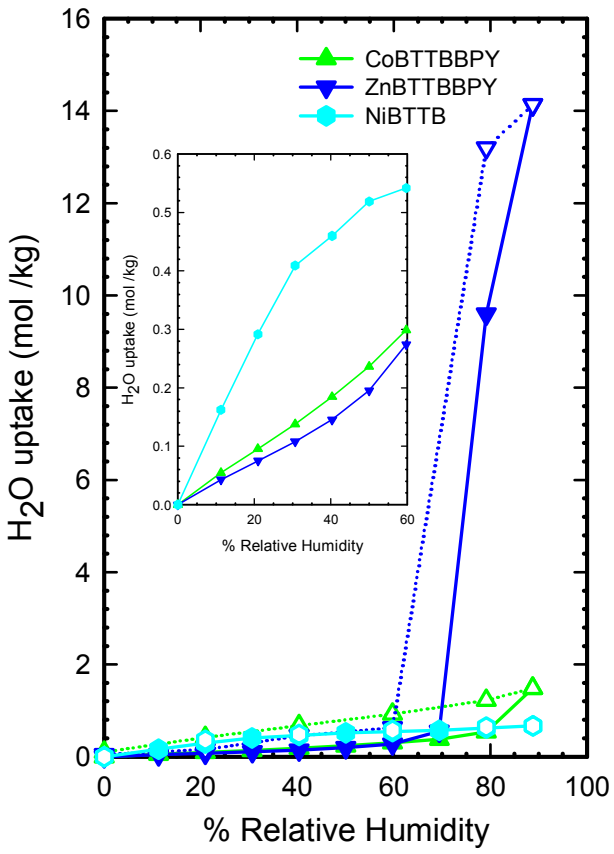

Fig. 4 Water vapor adsorption/desorption isotherms measured at 25 ˚C for desolvated compounds of CoBTTBBPY, ZnBTTBBPY, and NiBTTB (closed symbols: adsorption; open symbols: desorption). Lines connecting the adsorption points are to guide the eye.

this observation (Fig. S22, ESI)†. It has been previously reported that MOF-508 (ZnBDCBPY), which is a 2-fold interpenetrated MOF also showed similar hydrophobic character.[49] Therefore, the hydrophobicity of BPY-based MOFs is not surprising considering that the coordination environment of Zn or Co ions in these MOFs is identical to ZnBDCBPY. Additionally, all zinc or cobalt ions are coordinated to oxygen and nitrogen atoms of ligands, and there are no free coordination sites available for water to readily interact with. These BPY-based interpenetrated MOFs are stable even after exposure to 90% RH as discussed later (Table 1, Fig. 5) while ZnBDCDABCO (non-catenated) is stable only up to 30% RH[21] even though DABCO is more basic than BPY. One possible reason for stability of these BPY-based MOFs could be the 2-fold catenation (interpenetration/ interweaving) as catenated crystal structures are expected to be more stable.[50] Due to similar reasons, MOFs such as MOF-508[49] and SNU-80[51] were also found to be water stable.

Figure 5 shows the PXRD patterns of activated, water vapor exposed, and regenerated samples of NiBTTB, CoBTTBBPY, and ZnBTTBBPY. Minimal changes in the PXRD patterns are observed indicating that these three materials are stable even after exposure to 90% RH. Surface areas also remain unchanged for all the three samples after regeneration (Table 1). The hydrophobicity of these materials can ensure minimal wetting of the pores and therefore, capacities and selectivities for adsorptive gas separations can remain high. Since these MOFs maintain porosity and surface area after water vapour exposure, these materials can be classified as having good kinetic stability.

As both the CoBTTBAZPY and ZnBTTBAZPY MOFs are isostructural and have similar pore sizes, their water loadings are approximately the same (Fig. 6). The isotherms can be classified as type V according to IUPAC[48] classification, indicating that for these materials are surface adsorption is dominant at lower relative humidities while pore filling commences at higher relative humidities.[52,53]. The amount of water vapor adsorbed increases gradually with increase in relative humidity up to 40% RH. In the higher humidity region, the water loading increases sharply. This is probably the result of condensation of water in the pores. The water vapor capacities at 90% RH are 12.3 mol/kg (22.1 wt%) for CoBTTBAZPY and 10.8 mol/kg (19.3 wt%) for ZnBTTBAZPY. The water vapor isotherms of both the MOFs are irreversible and exhibit large hysteresis which indicates structural change upon water exposure.[21,22] The hysteresis is larger in CoBTTBAZPY compared to ZnBTTBAZPY and that is why CoBTTBAZPY shows higher degradation (Table 1). Moreover, it can be seen that a small amount of water is retained in the pores at 0% RH during desorption. This suggests that water molecules are strongly bound in these MOFs unlike BPY-based pillared MOFs. Most likely, free nitrogen sites (azo group) enhance the affinity of both these MOFs towards the polar water molecules.

The XRD patterns after water adsorption experiments and regeneration (Fig. 7) still show some of the initial XRD peaks, but other peaks have disappeared, indicating loss of crystallinity and partial collapse of the structure. The N_2 adsorption isotherms of these AZPY-based MOFs are measured again after regeneration. BET surface area loss is 56 % for CoBTTBAZPY and 43 % for ZnBTTBAZPY (Table 1). It is interesting to note that by merely changing the pillar linker from BPY to AZPY, the water stability of Co/Zn-based pillared MOFs has reduced significantly. The reason proposed for the water stability of BPY-based pillared MOFs is the 2-fold catenation present in them.[49]

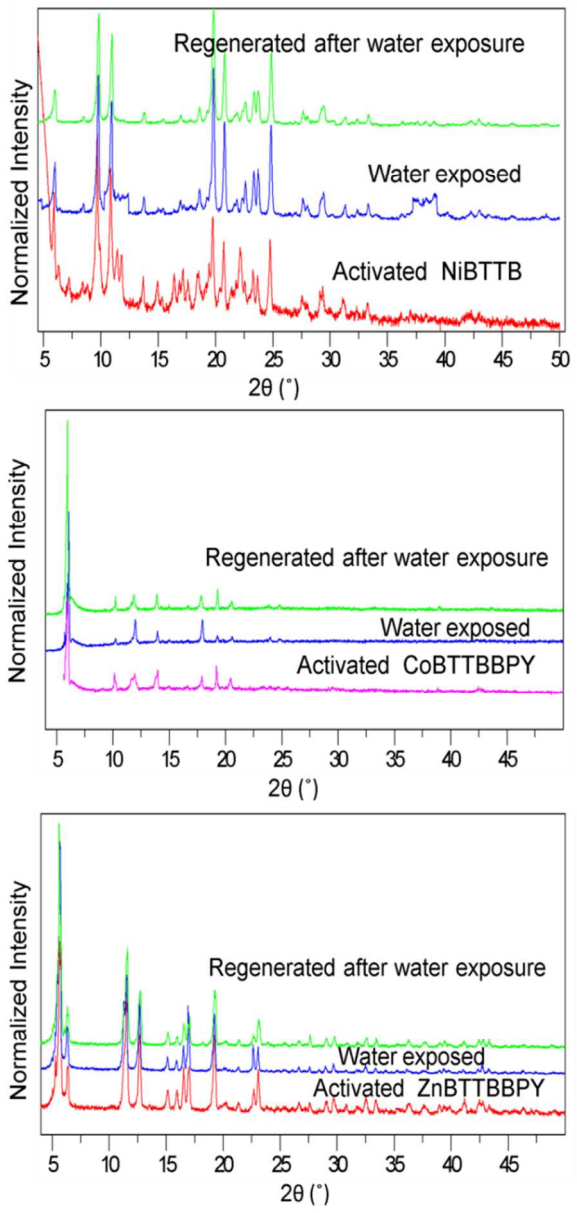

Fig. 5 Powder X-ray diffraction patterns of activated, water exposed, and regenerated NiBTTB, CoBTTBBPY, and ZnBTTBBPY.

Farha and Hupp have shown that formation of non-catenated pillared MOFs require either a sterically demanding or hydrogen-bonding capable dipyridyl ligand.[7] Hence, we propose that the AZPY-based pillared MOFs reported here has a smaller degree of catenation compared to BPY-based pillared MOFs because the azo group is H-bonding capable. This explanation is well supported by their lower thermal stability compared to BPY-based pillared MOFs (Table 1). Moreover, larger pores and free nitrogen sites in AZPY-based pillared MOFs enhance the interactions between the framework and water molecules and thus, permits organized clustering of water molecules to occur readily, leading to the framework collapse. Furthermore, higher rotational effects[37] of AZPY ligand compared to BPY can also contribute to the instability observed here. However, we still observe that mixed ligand MOFs made from BTTB and N-based pillar ligands (BPY, AZPY) are more stable than single ligand MOFs (e.g. CdBTTB, ZnBTTB) made from BTTB. NiBTTB is an exception due to its 2D net structure and 1D pore channels which limit the diffusion of water molecules. Moreover, Ni^{2+} has the lowest standard reduction potential among the metals used here and hence, it is less prone to react with water.[32] The greater stability of pillared MOFs is attributed to the higher basicity of the N-based pyridyl linkers which in turn leads to stronger metal-ligand bonds.[25,26]

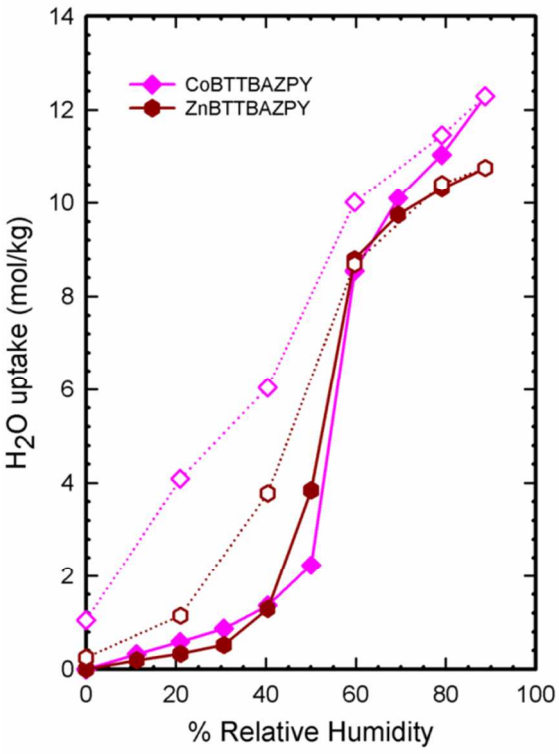

Fig. 6 Water vapor adsorption/desorption isotherms measured at 25 ˚C for desolvated compounds of CoBTTBAZPY and ZnBTTBAZPY (closed symbols: adsorption; open symbols: desorption). Lines connecting the adsorption points are to guide the eye.

4. Conclusions

The water stability of the BTTB-based MOFs is investigated by conducting water vapor adsorption experiments and subsequent structural analysis. The crystal structures of ZnBTTB and CdBTTB have completely degraded after water exposure. Instability of ZnBTTB is attributed to the four-coordinated zinc carboxylate system. Similarly, CdBTTB is also not stable as Cd^{2+} ions possess a coordination number of 4 in the activated (desolvated) form of MOF. ZnBTTBBDC has not degraded significantly after water exposure in contrast to CdBTTB and ZnBTTB. This could be attributed to high metal coordination number and high nuclearity of Zn ions in the SBU. ZnBTTBBPY, CoBTTBBPY and NiBTTB show hydrophobic nature compared to other BTTB-based MOFs. Hydrophobicity of BPY-based pillared MOFs is due to absence of any hydrophilic sites while NiBTTB is hydrophobic because of 2D net structure and 1D pore channels which limit the diffusion of water molecules. AZPY-

Journal of Materials Chemistry A

Dynamic Article Links ►

Cite this: DOI: 10.1039/c0xx00000x

www.rsc.org/xxxxxx

ARTICLE TYPE

based pillared MOFs show ~ 50% loss in surface area after water exposure while BPY-based pillared MOFs remain stable. Instability of AZPY-based MOFs could be attributed to a lesser extent of catenation, higher rotational effects of AZPY ligand, clustering of water molecules due to larger pores, and strong interactions between water molecules and free nitrogen sites. Understanding the factors that contribute to stability or instability of MOFs in the presence of water vapour is important for developing MOF applications. This work reports a systematic study which further addresses structural features of MOFs that considerably impact their use in moisture-sensitive industrial and commercial applications.

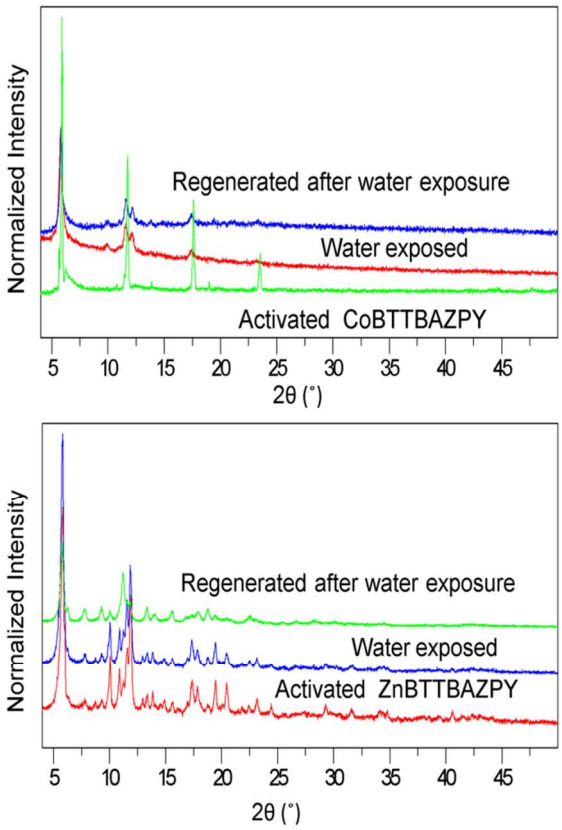

Fig.7 Powder diffraction patterns of activated, water exposed, and regenerated CoBTTBAZPY and ZnBTTBAZPY.

Acknowledgements

This work supported by the National Science Foundation under CBET grant number 1009682 and the Department of Defense under PECASE award W911NF-10-1-0079.

References

1 G. Ferey, *Chem. Soc. Rev.* 2008**, 37 (1)**, 191-214.
2 S. J. Garibay and S. M. Cohen, *Chem. Commun.* 2010**, 46 (41)**, 7700-7702.
3 G. Ferey, C. Mellot-Draznieks, C. Serre and F. Millange, *Acc. Chem. Res.* 2005**, 38 (4)**, 217-225.
4 H. C. Zhou, J. R. Long and O. M. Yaghi, *Chem. Rev.* 2012, **112**, 673-674.
5 J. L. C. Rowsell and O. M. Yaghi, *J. Am. Chem. Soc.* 2006, **128**, 1304-1315.
6 T. R. Cook, Y. R. Zheng and P. J. Stang, *Chem. Rev.,* 2013, **113 (1)**, 734–777.
7 O. K. Farha and J. T. Hupp, *Acc. Chem. Res.* 2010, **43**, 1166-1175.
8 K. K. Tanabe and S. M. Cohen, *Chem. Soc. Rev.* 2011, **40**, 498-519.
9 M. Eddaoudi, J. Kim, N. Rosi, D. Vodak, J. Wachter, M. O'Keeffe and O. M. Yaghi, *Science* 2002, **295**, 469-472.
10 G. Ferey, *Dalton Trans*. 2009, **23**, 4400-4415.
11 R. J. Kuppler, D. J. Timmons, Q. R. Fang, J. R. Li, T. A. Makal, M. D. Young, D. Q. Yuan, D. Zhao, W. J. Zhuang and H. C. Zhou, *Coord. Chem. Rev.* 2009, **253**, 3042-3066.
12 S. Kitagawa, R. Kitaura and S. Noro, *Angew. Chem.-Int. Ed*. 2004, **43**, 2334-2375.
13 K. Sumida, D. L. Rogow, J. A. Mason, T. M. McDonald, E. D. Bloch, Z. R. Herm, T.-H. Bae and J. R. Long, *Chem. Rev.* 2011, **112**, 724-781.
14 J. R. Li, R. J. Kuppler and H. C. Zhou, *Chem. Soc. Rev.* 2009, **38**, 1477-1504.
15 J. R. Karra and K. S. Walton, *Langmuir* 2008, **24**, 8620-8626.
16 U. Mueller, M. Schubert, F. Teich, H. Puetter, K. Schierle-Arndt and J. Pastre, *J. Mater. Chem.* 2006, **16**, 626-636.
17 S. Keskin, T. M. van Heest and D. S. Sholl, *ChemSusChem* 2010, **3**, 879-891.
18 N. C. Burtch, H. Jasuja, D. Dubbeldam and K. S. Walton, *J. Am. Chem. Soc.* 2013, **135**, 7172-7180.
19 Y.Wang and M. D.Levan, *J. Chem. Eng. Data* 2009, **54** , 2839.
20 Y.Li and R. T.Yang, *Langmuir* 2007, **23**, 12937.
21 Z. J. Liang, M. Marshall and A. L. Chaffee, *Microporous Mesoporous Mater.* 2010, **132**, 305.
22 A.Kondo, T. Daimaru, H. Noguchi, T. Ohba, K. Kaneko and H. Kanob, *J. Colloid and Interface Sci.* 2007, **314**, 422.
23 P. Kusgens, M. Rose, I. Senkovska, H. Frode, I. A. Hensche, S. Siegle and S. Kaskel, *Microporous Mesoporous Mater.* 2009, **120**, 325.
24 P. M. Schoenecker, C. G. Carson, H. Jasuja, C. J. J. Flemming and K. S. Walton, *Ind. Eng. Chem. Res.* 2012**, *51* (18)**, 6513-6519.
25 J. J. Low, A. I. Benin, P. Jakubczak, J. F. Abrahamian, S. A. Faheem and R. R. Willis, *J. Am. Chem. Soc.* 2009, **131**, 15834.
26 H. J. Choi, M. Dinca, A. Dailly and J. R. Long, *Energy Environ. Sci.* 2010, **3**, 117.
27 I. J. Kang, N. A. Khan, E. Haque and S. H. Jhung, *Chem. Eur. J.* 2011, **17**, 6437-6442.
28 S. M. Cohen, *Chem. Rev.* 2012, **112(2)**, 970-1000.
29 A. Schaate, S. Dühnen, G. Platz, S. Lilienthal, A. M. Schneider and P. Behrens, *Eur. J. Inorg. Chem.*2012, **5**, 790–796.
30 H. Jasuja, J. Zang, D. S. Sholl and K. S. Walton, *J. Phys. Chem. C* 2012, **116,** 23526-23532.
31 D. Feng, H.-L. Jiang, Y.-P. Chen, Z.-Y. Gu, Z. Wei, and H.-C. Zhou, *Inorg. Chem.* 2013, **52**, 12661−12667.
32 J. Liu, A. I. Benin, A. M. B. Furtado, P. Jakubczak, R. R. Willis and M. D. LeVan, *Langmuir* 2011, **27**, 11451-11456.
33 K. Tan, N. Nijem, P. Canepa, Q. Gong, J. Li, T. Thonhauser and Y. J. Chabal, *Chem. Mater.* 2012, **24**, 3153-3167.

34 H. Li, W. Shi, K. Zhao, H. Li, Y. Bing and P. Cheng, *Inorg. Chem.*, 2012, **51**, 9200–9207.
35 H. Jasuja, Y. G. Huang and K. S. Walton, *Langmuir*, 2012, **28**, 16874–16880.
36 H. Jasuja, N. C. Burtch, Y. G. Huang, Y. Cai and K. S. Walton, *Langmuir* 2013, **29**, 633-642.
37 J. B. DeCoste, G. W. Peterson, H. Jasuja, T. G. Glover, Y. G. Huang and K. S. Walton, *J. Mater. Chem. A* 2013, **1**, 5642-5650.
38 J. Yang, A. Grzech, F. M. Mulder and T. J. Dingemans, *Chem. Commun*. 2011, **47**, 5244-5246.
39 T. Wu, L. Shen, M. Luebbers, C. Hu, Q. Chen, Z. Ni and R. I. Masel, *Chem. Commun*. 2010, **46**, 6120-6122.
40 J. G. Nguyen and S. M. Cohen, *J. Am. Chem. Soc.* 2010, **132**, 4560.
41 Y. Cai, Y. D. Zhang, Y. G. Huang, S. R. Marder and K. S. Walton, *Cryst. Growth Des.* 2012, **12**, 3709-3713.
42 C. Serre, *Angew. Chem. Int.* Ed. 2012, **51**, 6048-6050.
43 J. M. Taylor, R. Vaidhyanathan, S. S. Iremonger and G. K. H. Shimizu, *J. Am. Chem. Soc.* 2012, **134**, 14338-14340.
44 N. C. Burtch, H. Jasuja and K. S. Walton, *Chem. Rev.* 2014 (In press, DOI: 10.1021/cr5002589).
45 O. K. Farha, C. D. Malliakas, M. G. Kanatzidis and J. T. Hupp, *J. Am. Chem. Soc.* 2010, ***132***, 950.
46 J. R. Karra, Y. Huang and K. S. Walton, *Cryst. Growth Des.* 2012, **13 (3)**, 1075-108.
47 K. S. Walton and R. Q. Snurr, *J. Am. Chem. Soc.* 2007, **129**, 8552-8556.
48 E. P. Ng and S. Mintova, *Microporous Mesoporous Mater.* 2008, **114**, 1.
49 H. Jasuja and K. S. Walton, *Dalton Trans.* 2013, **42**, 15421-15426.
50 J. Zhang, L.Wojtas, R. W. Larsen, M. Eddaoudi and M. J. Zaworotko, *J. Am. Chem. Soc.* 2009**, 131 (47)**, 17040-+.
51 L.-H. Xie and M. P. Suh,*Chem.–Eur. J.*, 2011, **17**, 13653–13656.
52 J. S. Oh, W. G. Shim, J. W. Lee, J. H. Kim, H. Moon and G. J. Seo, *Chem. Eng. Data* 2003, **48**, 1458.
53 J. C. Liu and P. A. Monson, *Langmuir* 2005, **21**, 10219.

Journal of Materials Chemistry A Dynamic Article Links ►

Cite this: DOI: 10.1039/c0xx00000x

www.rsc.org/xxxxxx

ARTICLE TYPE

Table 1. BET Surface Areas Before and After Water Adsorption for all the MOFs Synthesized in this Work

MOF	Pore size (Å)	Pore volume (cm^3/g)	BET surface area (m^2/g)	Activation process (under vacuum)	Thermal stability	Features	BET surface area (after 90% RH)	Change in surface area (%)
CdBTTB	5.413	0.19	415	300 ˚ C (1h)	350 ˚C	3-D pore system, open Cd sites	0	100
ZnBTTB	4.468	0.251	447	250 ˚ C (2h)	300 ˚C	3-D pore system, interpenetrated	0	100
ZnBTTBBDC	4.243	0.209	441	250 ˚ C (1h)	350 ˚C	2-D pore system, open Zn sites	220	50
NiBTTB	4.291	0.2	391	Chloroform Exchange and 120 ˚ C (12h)	350 ˚C	1-D pore system, open Ni sites	391	0
CoBTTBBPY	4.064	0.396	843	Chloroform Exchange and 120 ˚ C (12h)	400 ˚C	2-D pore system, interpenetrated	843	0
ZnBTTBBPY	4.064	0.38	841	Chloroform Exchange and 120 ˚ C (12h)	350 ˚C	2-D pore system, interpenetrated	841	0
CoBTTBAZPY	4.942	0.389	805	Chloroform Exchange and 120 ˚ C (12h)	300 °C	3-D pore system, interpenetrated	356	56
ZnBTTBAZPY	4.942	0.357	647	Chloroform Exchange and 120 ˚ C (12h)	300 ˚C	3-D pore system, interpenetrated	370	43

TOC Graphic